Supplementary Material

Supplementary A: Additional country-wide results and discussion

The figures S1 – S5 describe the development of the state of Finnish forests in different harvest scenarios. We show the results relative to the baseline scenario. After first ca. 20 years, forest increment increased in all harvest scenarios higher than baseline, while decreased in the scenario with harvests lower than the baseline (Fig. S1). This result indicates that in our analysis baseline scenario with harvests of 65% of current annual increment (CAI) leads to the ageing of forests and thus lowering trend of growth and yield. For the comparison, the dashed line in the Fig. S1 shows the increment simulated by PREBAS model (Valentine and Mäkelä, 2005, Peltoniemi et al. 2015, Minunno et al. 2016, Minunno et al. 2019) with harvest scenario of 100 mill.m^3 $year^{-1}$ which is close to our 100% harvest scenario. PREBAS is a semi-empirical model that predicts forest carbon balances and growth in annual time step based on daily estimates of gross primary production coupled to the evapotranspiration and water balance of the stand. Through to the theoretical rules describing the structure and growth of the trees (Valentine and Mäkelä 2005, Mäkelä et al. 2016) biomass allocation between tree compartments are predicted and stand level carbon balances estimated.

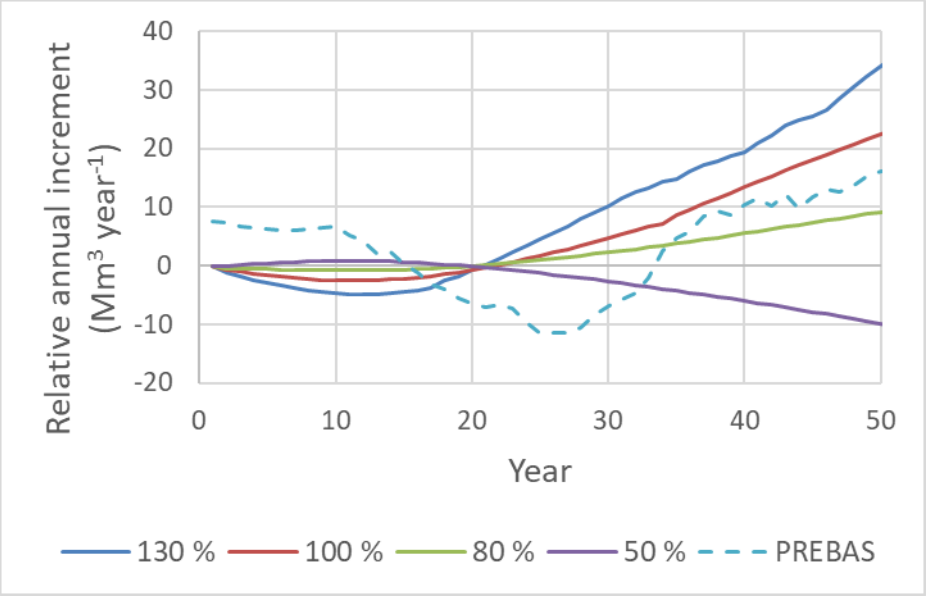

Supplementary Figure S1 Difference in annual stem volume increment between the baseline (65% of current annual increment, CAI) and each harvest scenario.

Different harvest levels resulted in large differences forest age structure (Fig. S2). The proportion of the oldest age class was over 40% in the lowest harvest scenario in average during the 50 years analysis time span, while four oldest classes had only 13% together in the highest harvest scenario. Despite the decreasing increment the highest growing stock was reached in the lowest harvest scenario being over 500 mill.m^3 higher than in baseline scenario after 50 years (Fig. S3). In the highest harvest scenario the growing stock was almost 2500 mill.m^3 smaller at the end of analysis than in baseline. The growing stock decreased over 1000 mill.m^3 in the highest scenario from the initial state. In the 100% harvest scenario, the growing stock was ca. 500 mill.m^3 smaller after 50 years than in the initialization. This result demonstrates that harvests corresponding CAI (100% scenario) are not sustainable in terms of growing stock and carbon storage although same harvest level was sustained during 50 years.

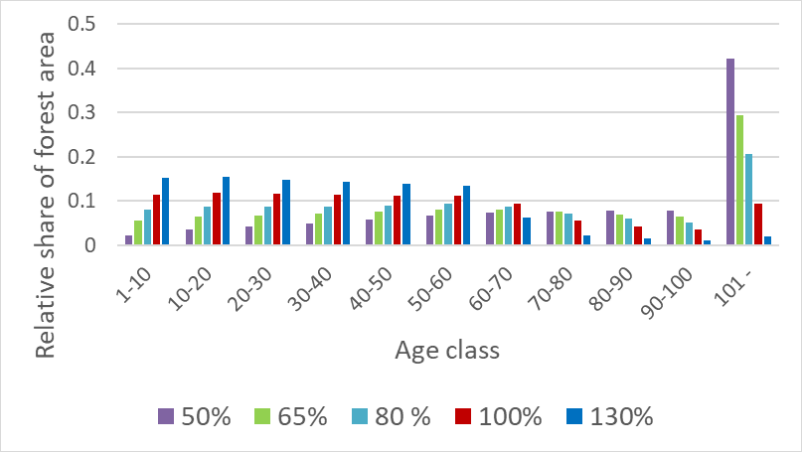

Supplementary Figure S2 Age structure of forests in the baseline scenario (65% of current annual increment, CAI) and in different harvest scenarios. Values are the averages of the simulated 50 years.

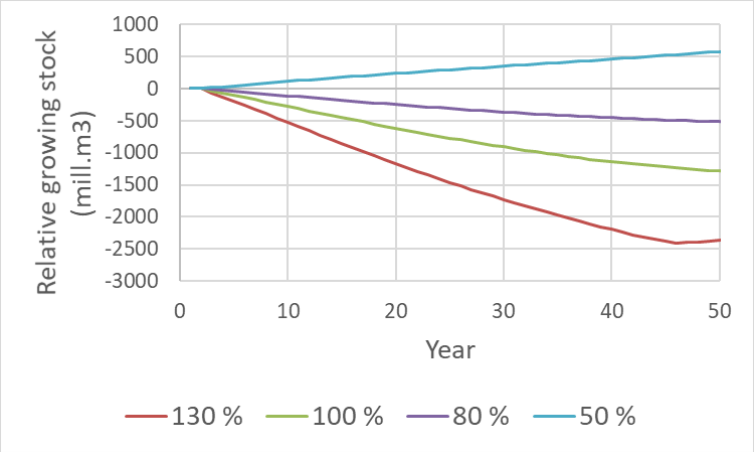

Supplementary Figure S3 The development of volume of growing stock harvest scenario minus the baseline scenario (65% of current annual increment, CAI).

The highest harvest level could be sustained 40 years in our analysis. After that period, the pursued harvest could not be reached due to lack of harvestable growing stock but harvest level decreased ca. 40 mill.m^3, i.e. almost 20 mill. m^3 lower level than in 100% scenario (Fig. S4). Harvest level recovered slightly, ca. 5 mill. m^3, during next ten years, but remained clearly on the lower than in sustained 100% harvest scheme. In the lowest harvest scenario, harvesting exceeded the preset target level during almost whole 50 years . This was due to the forced thinnings at stand level forest management in MOTTI simulations when silvicultural recommendations were followed in the simulations. These forced thinnings also resulted in that volume removed in final harvests/clearcuts in this scenario was very low, only ca. 5 mill. m^3 $year^{-1}$ in average.

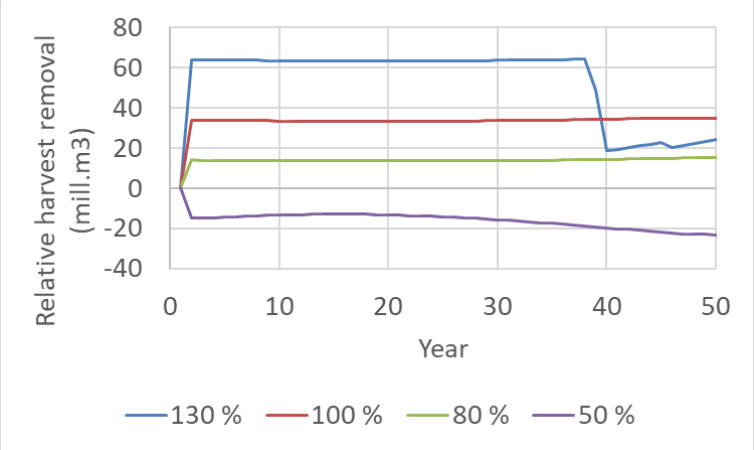

Supplementary Figure S4 The difference of annual harvests between the baseline scenario (65% of current annual increment, CAI) and each harvest scenario.

The ageing of forests in the baseline and lowest harvest scenario led also to the increased size of trees. This was indicated by log:pulpwood ratio in our analysis (Fig. S5). This ratio decreased in

relative terms in all scenarios harvesting more than baseline but only in the highest harvest scenario the sawlog:pulpwood ratio decreased in absolute terms compared with the initial state.

We used initial state of forests, baseline scenario harvest level, species specific timber assortment information (Table S1) and product portfolio (Table 2) in the estimation of harvest wood product volume in the first year of the simulation. With this volume and product lifetime curves (Fig. S10) we performed spin-off simulation in order to reach the equilibrium state of harvested wood products (HWP) carbon storage. We used this equilibrium value as an initialization value for the actual harvest scenarios and calculated the carbon storage of HWP within each scenario (Fig. S6). From these values we calculated the annual carbon stock change of HWPs.

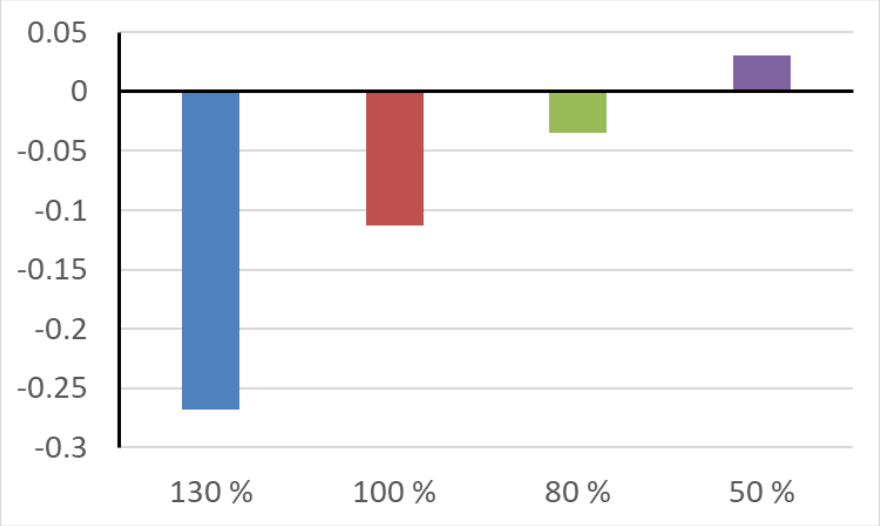

Supplementary Figure S5 The average difference of growing stock sawlog:pulpwood ratio between the baseline (65% of current annual increment, CAI) and each harvest scenario in 50 years simulation period. Positive values mean higher share of logs, negative values mean higher pulpwood share than in baseline.

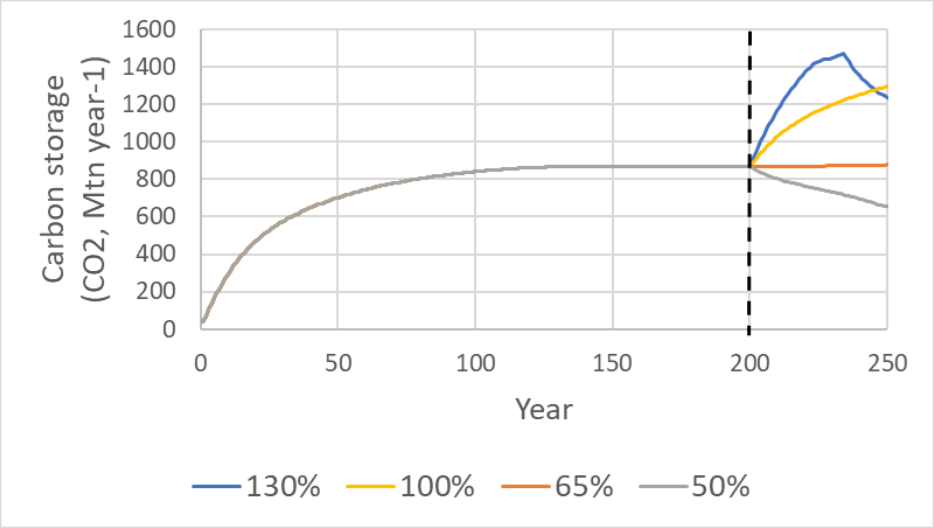

Supplementary Figure S6 Development of carbon storage of harvested wood products (HWP) in the spin-off simulation and in actual scenarios. The dashed vertical line shows the starting point of the actual scenarios.

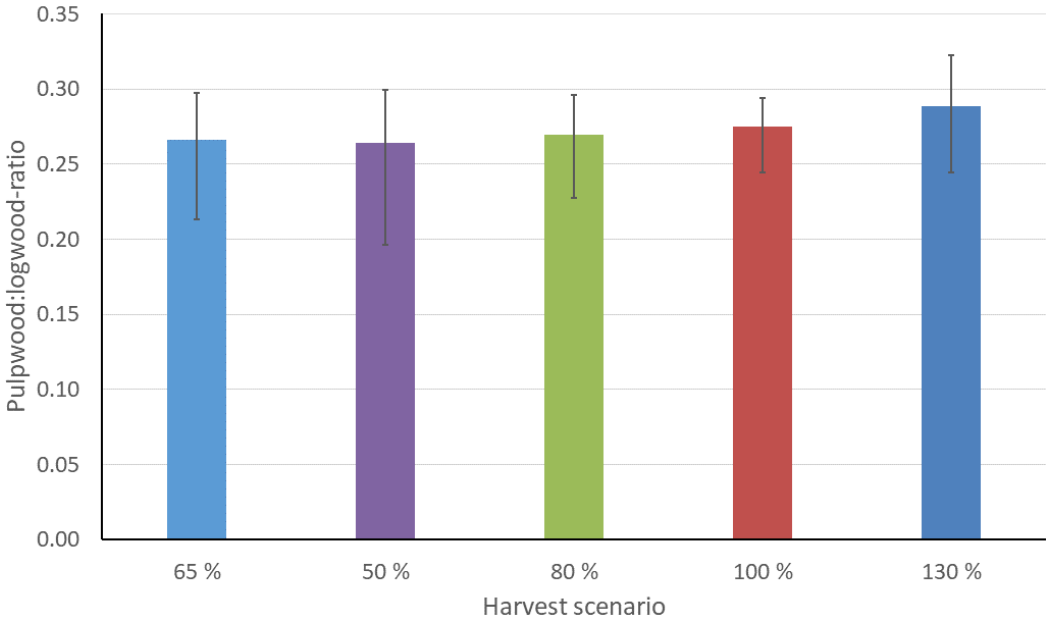

Supplementary Figure S7 The average pulpwood:sawnwood ratio in harvested wood of 50 years in different harvest scenarios. Error bars shows the difference between minimum and maximum estimate of the variable during simulation.

Figure S8 describes the effect of harvested wood allocated to different wood products on radiative forcing (RF) in different harvest scenarios. We did two different simulations where all harvest wood was treated either as sawnwood or as pulpwood. Specifically this means that total harvested wood volume decayed either according to the curves of sawnwood products or curves of pulpwood products (see Fig. S10), and the amount of avoided emissions due to wood use is calculated either solely with displacement factors (DF) of sawnwood or pulpwood. In this analysis, we used average displacement factor values of 0.913, 0.905, and 0.819, for sawnwood of Scots pine, Norway spruce and silver birch, respectively. For pulpwood products we used DF value 0.695.

This analysis explicitly shows the significance of the product allocation to different commodities, e.g. in 80% scenario, when all HWPs decayed as sawnwood then RF corresponded that of 65% scenario (lower yellow dashed line follows black dotted line). Similarly, when all HWPs decayed as pulpwood products in 50% scenario the RF corresponded again 65% scenario.

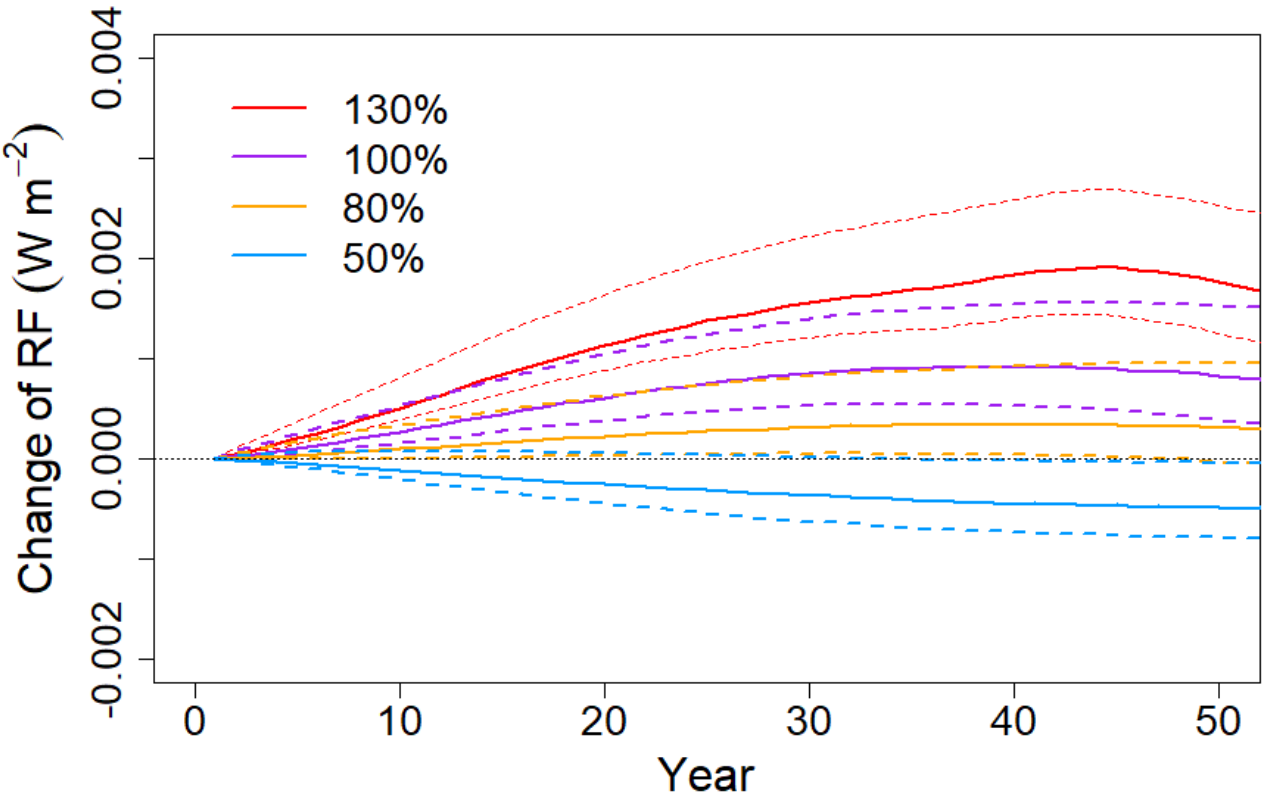

Supplementary Figure S8 The annual difference of the global radiative forcing (RF) between each scenario and the baseline (65% of current annual increment, CAI), in the current climate including carbon in trees, soil and harvested wood products (HWP), and avoided emissions due to the wood use. Different colors represent varying harvest levels given as a percentage of present CAI in Finland. Constant lines correspond Fig. 4b curves while dashed lines describes two extremes i.e. if all HWP would have decay curves of sawnwood or all HWP would have decay curves of pulpwood.

References

Mäkelä, A., Pulkkinen, M., Mäkinen, H. Bridging empirical and carbon-balance based forest site productivity – Significance of below-ground allocation. For. Ecol.Manage. 372, 64–77, 2016, https://doi.org/10.1016/j.foreco.2016.03.059.

Minunno, F., Peltoniemi, M., Launiainen, S., Aurela, M., Lindroth, A., Lohila, A., Mäkelä, A. Calibration and validation of a semi-empirical flux ecosystem model for coniferous forests in the Boreal region. Ecol. Model. 341, 37–52, 2016, https://doi.org/10.1016/J.ECOLMODEL.2016.09.020.

Minunno, F., Peltoniemi, M., Härkönen, S., Kalliokoski, T., Mäkinen, H. and Mäkelä, A. Bayesian calibration of a carbon balance model PREBAS using data from permanent growth experiments and national forest inventory. Forest Ecology and Management 440, 208–257, 2019.

Peltoniemi, M., Pulkkinen, M., Aurela, M., Pumpanen, J., Kolari, P. and Mäkelä, A.: A semi-empirical model of boreal forest gross primary production, evapotranspiration, and soil water – calibration and sensitivity analysis, Bor. Env. Res., 20, 151-171, 2015.

Valentine, H.T., Mäkelä, A. Bridging process-based and empirical approaches to modeling tree growth. Tree Physiol. 25 (7), 769–779, 2005. http://www.ncbi.nlm.nih.gov/pubmed/15870047.

Supplementary B: Additional stand level analyses and results

B1 Carbon dynamics of forest stand and harvested wood products

The single stand simulator MOTTI is an empirical stand-level analysis tool and decision support system for forest management (Salminen et al. 2005). MOTTI simulations were done for all species and site fertility classes from regeneration to age 110 years applying national forest management recommendations (Recommendations for…2006) (Fig.S9). This entailed using regeneration by planting with species and fertility-class specific density (saplings ha^{-1}). Thereafter, the tending of saplings, pre-commercial thinning, commercial thinnings and final harvest was performed according to the recommendations. The timing of the pre-commercial thinning was based on the species and fertility-class specific tree height while the timing of the commercial thinning depended on basal area. Whenever a species and fertility-class specific basal area limit was crossed, a thinning from below was performed. The treatment intensity was defined on the basis of the basal area in such a way that removal of trees decreased the stand basal area to the recommended level. In the first commercial thinning, the opening of strip roads was mimicked by removing 18 % of the stand basal area. The timing of final harvest was based on either stand age or stand mean diameter depending on which factor was filled first (Fig. S9, Table 1). Final harvest was done as a clear cut with shortwood logging system, in which trees are topped, limbed and stems cut to the pre-defined lengths at the harvesting site. The surface area of newly established stands after regeneration on the Herb-rich sites were evenly divided between silver birch and Norway spruce in the simulations while on the other site types it was assumed that stands regenerate with the same species as in previous generation. Having carried out the simulations for all species and site fertility classes, the temporal development of stem volume was assigned for each 10-year age classes, defined as the mean simulated volumes of each age class. The resulting age class tables were used for creating the transition of state for all

species and fertility classes as explained above. Forest growth and yield in each age class followed the South-Finland conditions because BVOC-SOA connection to stand development is determined only in South-Finland. The MOTTI simulator produces the harvested volume of logs and pulpwood in both the thinnings and final harvest (Table S1), which allows us to compute the amounts of roundwood assortments (Fig. S10) and thereafter to calculate avoided emissions due to material and energy substitution. In the simulations we didn't consider whole tree harvesting for energy wood, i.e. harvesting residues were left at the site.

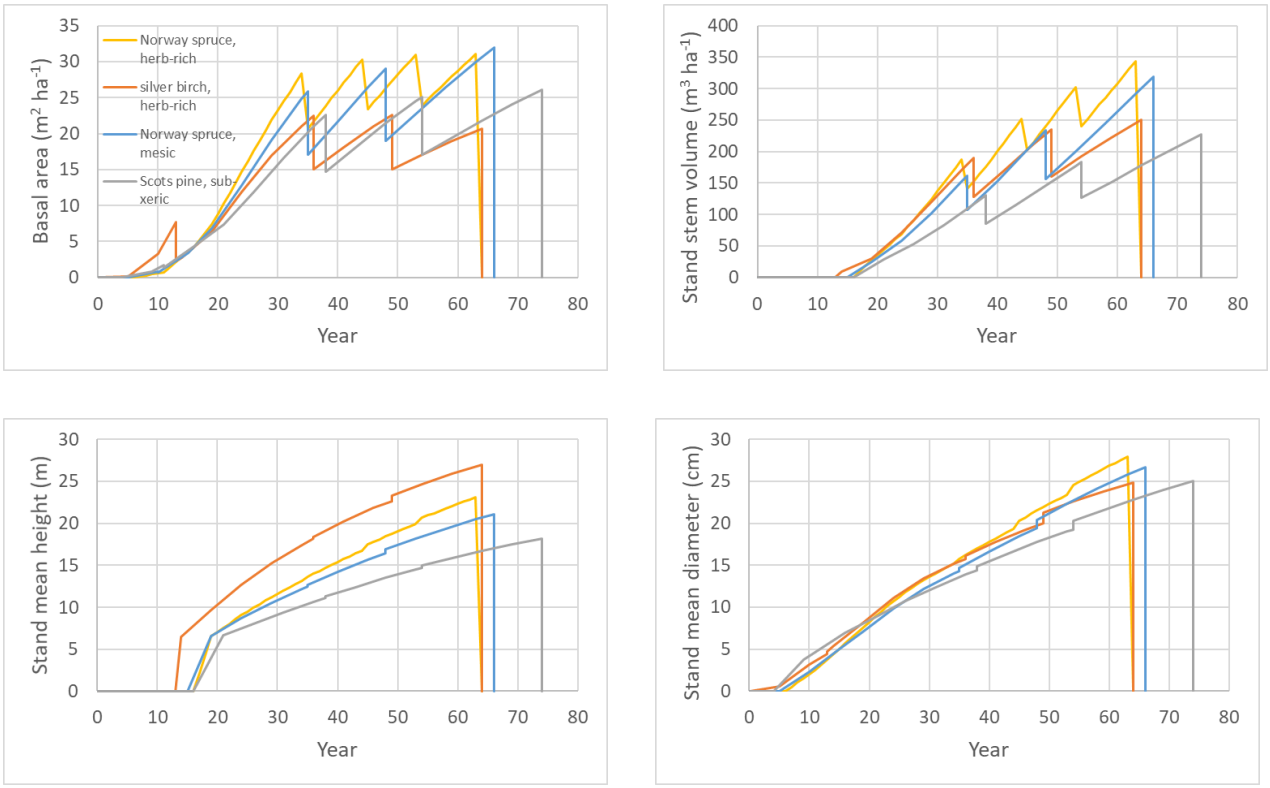

Supplementary Figure S9 Stand dynamics as simulated by MOTTI with Tapio recommendations. In the classification of Cajander (1949) the site fertility is determined based on the understorey vegetation. In this analysis, herb-rich corresponds fertile Oxalis-Myrtillus (OMT) site type, mesic is medium fertile Myrtillus (MT), and sub-xeric infertile Vaccinium-Myrtillus (VT).

Supplementary Table S1 Silvicultural recommendations (Recommendations for…2006) implemented in MOTTI stand simulator and applied in scenario simulations. Site types same as in Fig.S9.

Silvicultural treatment	Tree species silver birch	Norway spruce	Scots pine
Forest type/site fertility	Herb-rich	Herb-rich/Mesic	Sub-xeric
Regeneration type	Planting	Planting	Planting
Regeneration density	1600 trees ha^{-1}	1600-1800 trees ha^{-1}	1800-2000 trees ha^{-1}
Sapling tending	Yes	Yes	Yes
Pre-commercial thinning			
height	4-7 m	3-4 m	5-7 m
density after thinning	1600 trees ha^{-1}	1600-1800 trees ha^{-1}	1800-2000 trees ha^{-1}
First commercial thinning			
height	14-16 m	12-16 m	13-15 m
density after thinning	700-800 trees ha^{-1}	900-1000 trees ha^{-1}	900-1000 trees ha^{-1}
Second commercial thinning			
age	50 years	50 years	55 years
basal area before	22 m^2 ha^{-1}	28 m^2 ha^{-1}	25 m^2 ha^{-1}
basal area after	15 m^2 ha^{-1}	19 m^2 ha^{-1}	17 m^2 ha^{-1}
Final harvesting			
age	65-90 years	67-90 years	75-90 years
diameter	28-32 cm	22-28 cm	23-28 cm

Supplementary Table S2 Harvested wood products in different stands predicted by MOTTI-model.

ForestType	Species	Year of harvest	Logs (m^3 ha^{-1})	Pulpwood (m^3 ha^{-1})
Sub-xeric	Pine	40	1.4	40
		56	11	44
		76	149	74
Mesic	Spruce	37	2.3	47
		50	23	51
		68	253	61
Herb-rich	Spruce	35	7.6	47
		45	18	43
		54	42	31
		64	270	71
Herb-rich	Birch	38	1.6	56
		51	5.6	66
		66	83	162

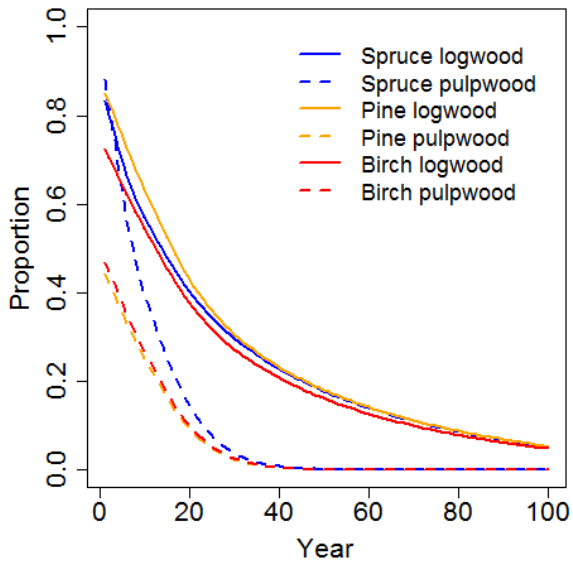

Supplementary Figure S10 Decay curves of wood products based on Karjalainen et al. (1994).

References

Cajander, A.K. 1949. Forest types and their significance. Acta Forestalia Fennica 56. 71 p.

Karjalainen, T., Kellomäki, S. and Pussinen, A.: Role of wood-based products in absorbing atmospheric carbon, Silva Fenn., 28, 67-80, 1994.

Salminen, H., Lehtonen, M. and Hynynen, J.: Reusing legacy FORTRAN in the MOTTI growth and yield simulator, Comput. Electron. Agric., 49, 103-113, 2005.

B2 Calculation of direct and indirect effects of aerosols

B2.1 Set-up of the SOSAA model

The 1D model SOSAA (Boy et al. 2011, Zhou et al. 2014) consists of 4 modules; (1) meteorology, (2) BVOC emissions, (3) gas-phase chemistry, and (4) aerosol dynamics. We simulated all atmospheric processes (meteorology, chemistry and aerosol dynamics) in 51 horizontally orientated layers. The height of the layers was fixed, with a logarithmical increase from ground up to 3 km. Around 20 of these layers were defined inside the forest canopy, thus the emissions of BVOCs was simulated in those layers where needles/leaves were allocated. Due to absence of measurements, we did not include BVOC emissions from other tree organs than the needles/leaves. The SOSAA code is written in Fortran90 and is parallelized, thus it can be executed on a supercomputer with a reasonable run-time. Since SOSAA is a column model, it assumes horizontally homogeneity. The consequence of this is that simulations are carried out for the individual tree stand with the assumption that the gas- and particle phase compounds from one stand does not interact with another stand.

Boundary layer meteorology in SOSAA

The meteorological transport is based on the coupled plant- atmosphere boundary layer model SCADIS (Sogachev et al. 2002, 2005, 2006, 2012). SCADIS is based on the Reynolds averaged Navier-Stokes equations for turbulent flow (Pope 2000). Turbulent fluxes are expressed as the product of a turbulent diffusion coefficient and the gradient of a mean quantity according to the concept first proposed by Boussinesq (Pielke 2002). Temperature, humidity and wind speed at the upper boundary of the model column were constrained by data from the ECMWF Interim Reanalysis database. The modeled temperature, humidity and wind speed were nudged towards the measurements conducted at several levels inside and above the canopy, between the surface and 72 m. The most important equations are provided in Boy et al. (2011), while updates and validations are presented in Mogensen et al. (2015).

Emissions of BVOCs in SOSAA

The emissions of organic vapors from the canopy are calculated by a modified version of MEGAN 2.04 (Model of Emissions of Gases and Aerosols from Nature (Guenther et al. 2006, Smolander et al. 2014). The estimated emissions are highly dependent on meteorological factors (temperature and light), leaf area, biomass, and the emission potentials of individual organic compounds that are specific for individual tree species. The canopy characteristics for all tree stand simulations can be found in Extended Data, Table 2. The standardized emission potentials (SEPs) for pine were based

on continuous chamber measurements at the SMEAR II site and data from Hakola et al. (2006), while the distribution of emitted monoterpenes from pine was assumed to be the average chemotype presented in Bäck et al. (2012). We have used SEPs for spruce from Hakola et al. (2003), but also unpublished data (personal communication with Hannele Hakola in 2012). The emission from birch was calculated using the temperature-sum-based emission potential presented in Hakola et al. (2001), while the distribution of emitted monoterpenes from birch was based on Hakola et al. (1998).

Gas-phase chemistry in SOSAA

The chemical reaction equations for the model runs were selected from the Master Chemical Mechanism (http://mcm. leeds.ac.uk/MCM/) version 3.2 (Jenkin et al. 1997, 2012, Saunders et al. 2003). The model runs included 7465 reactions with a total of 1854 chemical species representing the complete reaction paths for isoprene, 2-methyl-3-buten-2- ol, limonene, beta-pinene, alpha-pinene, beta-caryophyllene, methanol, acetone, acetaldehyde, formaldehyde, methane and all relevant inorganic reactions. Furthermore, the first order reactions of alpha-farnesene and other identified monoterpenes than those we have the full chemistry path for (Δ3- carene, sabinene, camphene, ocimene, and other monoterpenes than those mentioned here) were included. Also, updated Criegee intermediate chemistry was included as in Boy et al. (2011). KPP - the Kinetic PreProcessor (Damian et al. 2002, Sandu and Sanders 2006) was used to translate the reaction equations into Fortran90 code that performs the time integration of the kinetic system. The chemistry module is constrained by the measured concentrations of O_3, SO_2, CO, NO, NO_2 and CH_4.

Aerosol dynamics in SOSAA

The aerosol dynamics module in the SOSAA model is based on the University of Helsinki Multicomponent Aerosol model (UHMA, Korhonen et al. 2004). The processes simulated include nucleation, condensation, coagulation, evaporation and deposition. Particle concentrations were simulated for 40 particle size ranges (size bins) from 2 nm to 1 μm. In the model, particles are assumed to be spherical and to consist initially of sulphuric acid, water, and organic compounds. The onset of low or semi-volatile organic vapor condensation onto the nanosize inorganic clusters is determined by the Nano-Köhler theory (Kulmala et al. 2004). We have assumed that the formation of SOAs occur according to the organic nucleation theory. The sum of the first stable oxidation products from reactions between OH and monoterpenes (alpha-pinene, beta- pinene, and limonene) were chosen as the nucleating compounds (see also Zhou et al. 2014). The nucleation rate (Jorg) is related to the concentrations of sulphuric acid (H_2SO_4) and oxidized organic vapors (org) as:

$$J_{org} = k_{org} * [H_2SO_4]*[org] \quad (1)$$

where k_{org} is the nucleation coefficient for the organic nucleation mechanism. Besides H_2SO_4, organic condensing vapors in the model were assumed as the lump sum of the first stable reaction products from OH, O_3 and NO_3 oxidation of monoterpenes (see also Zhou et al. (2014, 2015). The aerosol dynamics module was constrained by the aerosol condensational sink (CS) which is calculated based on the aerosol number size distribution measurements (Boy et al. 2011). The CS determines how rapidly molecules will condense onto preexisting particles. This module is initialized every midnight by the measured DMPS (Differential Mobility Particle Sizer) distribution in order to obtain a correct background aerosol number size distribution.

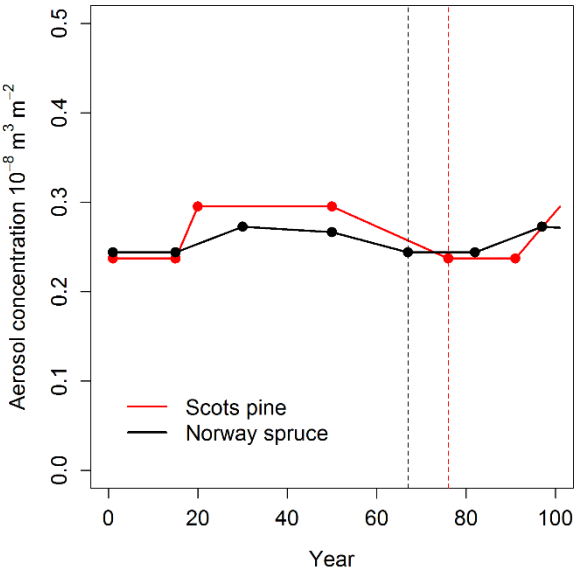

Supplementary Figure S11 The dynamics of boundary layer aerosols over 100 years in coniferous stands. The values are annual mean boundary layer aerosol volume burden provided for a 1 m^2 atmospheric column of 1 km high considering particles of sizes 1 nm – 1 µm. The dots are the stand ages where the biogenic volatile organic compounds and their effect on the aerosols was modeled (see Sect. 2.5 and Table 2). Lines are linear interpolations between dots. The starting point is bare land one year after clear cut (i.e. final harvest) and the vertical lines depict the year of next clear cut and the second rotation in different stands. We do not show values of silver birch here because we used ex-post calibration for radiative forcing of Secondary Organic Aerosols of birch (see suppl. B3)

Set-up for 2050 climate simulations by SOSAA

The daily weather for year 2050 was predicted using an emission scenario between RCP6.0 and RCP8.5 scenarios and the csriro_mk3_5 climate model. The simulated meteorological parameters in SOSAA were then nudged towards these predictions. We used the output from various climate models, in order to constrain SOSAA by the expected ambient concentrations of O_3, SO_2, CO, NO, NO_2 and CH_4 in year 2050. The predicted mole fractions of SO_2 and O_3 were obtained from GFDL-CM3 from the CMIP5 data archive (http://cmip-pcmdi.llnl.gov/cmip5/index.html). The predicted mole fraction of CH_4 was taken from CESM1-WACCM (from NCAR). There exists no predicted mole fractions of NO, NO_2 and CO for year 2050, thus we utilized the annual mean emission rates of NO and CO from IPCC RCP4.5. We assumed an identical change in the NO_2 concentration as in the NO concentration. This means that we have multiplied the 2010 measured concentrations with the following factors: O_3·1.0472, SO_2·0.3144, CO·0.3927, NO·0.2336, NO_2·0.2336, and CH_4·1.0562. We initialized the model with the same background aerosol concentrations as in current climate (year 2010) and likewise constrained the model with the same CS as in 2010.

B2.2 Details on the calculations of direct and indirect radiative aerosol effects

Direct radiative forcing calculation

The changes in direct radiative forcing (ΔDRF) from aerosols were calculated based on the method described in the supplementary material of Paasonen et al. (2013) and in the article by Lihavainen et al. (2009). Steps in calculation are listed below:

1. The monthly averaged aerosol volume burden Bv in the boundary layer was first calculated with the boundary layer height assumed as 1 km.

2. The change in the optical depth ($\Delta\tau$) between two simulations was then calculated by

$$\Delta\tau = \Delta Bv\ \rho\ Bsp$$

where $\rho = 1$ g cm^{-3} is the density of aerosols and Bsp = 3.9 m^2 g^{-1} is the mass extinction coefficient.

3. By assuming unity single scattering albedo for the aerosol, the monthly difference in aerosol direct forcing between two simulations was calculated using (Paasonen et al. 2013)

$$\Delta DRF = -(\Delta\tau)\beta S\Phi T_{at}^2(1-C_c)(1-R_s)^2$$

where β is the average upscatter fraction (assumed to be 0.3), S is the monthly mean daily solar insolation, Φ is the mean daytime value of the secant of the zenith angle, T_{at} is the atmospheric transmissivity (assumed as 0.76), R_s is the monthly mean surface albedo and C_c is the monthly mean fractional low cloud cover.

4. The final annual ΔDRF is the mean of the monthly ΔDRFs. In case of birch and spruce forest, the mean was made from the months available.

Besides the uncertainty associated with aerosol simulations, the main uncertainty in calculating ΔDRF in this method lies in the assumption of constant boundary layer height as 1000 m. In reality, the boundary layer height varies between ~200 m (night time) to 2000 m (day time), which contributes directly to the uncertainties of our results. Other sources of uncertainties are in the assumptions of the aerosol density, mass extinction coefficient, upscatter fraction and transmissivity. Mean surface albedo was assigned to each month by guessing between 0.3 (winter) – 0.1 (summer). The average monthly albedoes measured in Hyytiälä is between 0.322 – 0.1083 (see foot note below Table 1 in Kurtén et al. 2003). The monthly mean cloud cover fraction was calculated from ECMWF reanalyzed low cloud cover fraction, which contributes to the uncertainties too.

Calculation of aerosol indirect radiative forcing, i.e. cloud albedo effect.

The method is based on Kurtén et al. 2003.

1. CCN density N is assumed as 200 #/cm³.

2. The (SOSAA) simulated monthly mean concentration of particles over 80 nm is N1.

3. The pertubation of CCN particles formed from forest (N1) to the cloud albedo (ΔRc) is based on the linear form of Twomey's cloud sensitivity equation (Hobbs 1993, Twomey 1977):

$$\frac{\partial R_c}{\partial N} \approx \frac{\Delta R_c}{\Delta N} = \frac{R_c(1-R_c)}{3N}, \quad (3)$$

From which we obtain:

$$\Delta R_c = \frac{R_c(1-R_c)N_1}{3NAh} \quad (4)$$

4. The surface albedo (R_s) is estimated from January to December as [0.3 0.3 0.25 0.25 0.2 0.1 0.10.1 0.1 0.1 0.2 0.25]. Downward radiation and global radiation measurements are available from SMEAR II, but since these two measurements are made at different height, we did not apply them here. Surface albedo does not contribute a significant error in the whole calculation, when comparing to other source of errors.

5. The net albedo change caused by the CCN formed from forest (N1) is then calculated. Accounting for multiple reflections between the surface and clouds, the following expression was obtained for the total albedo Rtot (Sagan et al. 1979) and the total albedo difference ΔR_{tot}:

$$R_{tot} = R_c + \frac{R_s(1-R_c)^2}{1-R_cR_s} => \Delta R_{tot}$$

$$= \Delta R_c + R_s\left[\frac{[1-(R_c+\Delta R_c)]^2}{1-(R_c+\Delta R_c)R_s} - \frac{(1-R_c)^2}{1-R_cR_s}\right] \quad (5)$$

6. Monthly average low cloud cover (~1000m) CC in year 2010 is calculated from ECMWF reanalyzed data base. The average cloud cover is assumed unchanged in year 2050.

7. Daily solar insolation (S) in each month is estimated based on the equation given by Hartmann (1994). The location of Hyytiälä and mid-day of each month is used in the calculation.

8. Radiative forcing due to CCN from the forest (N1) is estimated for each month (i) by

$RF_i = S_i * c * \Delta R_{tot,i} * CC_i$

9. The annual mean is finally calculated by taking the mean of the monthly RF_i.

References

Bäck, J. et al. Chemodiversity of a Scots pine stand and implications for terpene air

concentrations. Biogeosciences 9, 689-702 (2012).

Boy, M. et al. Oxidation of SO2 by stabilized Criegee intermediate (sCI) radicals as a crucial source for atmospheric sulfuric acid concentrations. Atmos. Chem. Phys. 13, 3865-3879 (2013).

Damian, V., Sandu, A., Damian, M., Potra, F. & Carmichael, G. R. The kinetic preprocessor KPP - a software environment for solving chemical kinetics. Comput. Chem. Eng. 26, 1567-1579 (2002).

Guenther, A. et al. Estimates of global terrestrial isoprene emissions using MEGAN (Model of Emissions of Gases and Aerosols from Nature). Atmos. Chem. Phys. 6, 3181-3210 (2006).

Hakola, H. et al. Seasonal variation of mono- and sesquiterpene emission rates of Scots pine. Biogeosciences 3, 93-101 (2006).

Hakola, H. et al. Seasonal variation of VOC concentrations above a boreal coniferous forest. Atmos. Environ. 37, 1623-1634 (2003).

Hakola, H. et al. Variation of the VOC emission rates of birch species during the growing season. Boreal Environ. Res. 6, 237-249 (2001).

Hakola, H., Rinne, J. & Laurila, T. The hydrocarbon emission rates of tea-leafed willow (Salix phylicifolia), silver birch (Betula pendula) and European aspen (Populus tremula). Atmos. Environ. 32, 1825-1833 (1998).

Hartmann D. L. Global physical climatology (Academic Press, 1994).

Hobbs P. V. (ed.) Aerosol-cloud-climate interactions (Academic Press, 1993).

Jenkin, M. E., Saunders, S. M. & Pilling, M. J. The tropospheric degradation of volatile organic compounds: a protocol for mechanism development. Atmos. Environ. 12, 5275-5308 (1997).

Jenkin, M. E. et al. Development and chamber evaluation of the MCM v3.2 degradation scheme for β-caryophyllene. Atmos. Chem. Phys. 12, 5275-5308 (2012).

Korhonen, H., Lehtinen, K. E. J. & Kulmala, M. Multicomponent aerosol dynamics model UHMA: model development and validation. Atmos. Chem. Phys. 4, 757-771 (2004).

Kulmala M., Kerminen V.-M., Anttila T., Laaksonen A. & O'Dowd C.D. Organic aerosol formation via sulphate cluster activation. J. Geophys. Res. 109, D04205 (2004).

Kurtén, T. et al. Estimation of different forest-related contributions to the radiative balance using observations in southern Finland. Boreal Environ. Res. 8, 275-286 (2003).

Lihavainen, H. et al. Observational signature of the direct radiative effect by natural boreal forest aerosols and its relation to the corresponding first indirect effect. J. Geophys. Res. 114, D20206 (2009).

Mogensen, D. et al. Simulations of atmospheric OH, O3 and NO3 reactivities within and above the boreal forest. Atmos. Chem. Phys. 15, 3909-3932 (2015).

Pielke, R. Mesoscale meteorological modelling (Academic Press, San Diego, California, USA, 2002).

Paasonen P. et al. On the roles of sulphuric acid and low-volatility organic vapours in the initial steps of atmospheric new particle formation. Atmos. Chem. Phys. 10, 11223-11242 (2010)

Paasonen, P. et al. Warming-induced increase in aerosol number concentration likely to moderate climate change. Nature Geoscience 6, 438-442 (2013).

Pope, S. B. Turbulent Flows (Cambridge Univ. Press, UK, 2000).

Sagan C., Toon O. B. & Pollack J. B. Anthropogenic albedo changes and the Earth's climate. Science. 206, 1363-1368 (1979)

Sandu, A. & Sanders, R. Technical note: Simulating chemical systems in Fortran90 and Matlab with the Kinetic PreProcessor KPP-2.1. Atmos. Chem. Phys. 6, 187-195 (2006).

Saunders, S. M., Jenkin, M. E., Derwent, R. G. & Pilling, M. J. Protocol for the development of the Master Chemical Mechanism, MCM v3 (Part A): tropospheric degradation of nonaromatic volatile organic compounds. Atmos. Chem. Phys. 3, 161-180 (2003).

Smolander, S. et al. Comparing three vegetation monoterpene emission models to measured gas concentrations with a model of meteorology, air chemistry and chemical transport. Biogeosciences 11, 5425-5443 (2014).

Sogachev, A., Menzhulin, G., Heimann, M. & Lloyd, J. A simple three dimensional canopy - planetary boundary layer simulation model for scalar concentrations and fluxes. Tellus B. 54, 784-819 (2002).

Sogachev, A., Panferov, O., Gravenhorst, G. & Vesala, T. Numerical analysis of flux footprints for different landscapes. Theor. Appl. Climatol. 80, 169-185 (2005).

Sogachev, A. & Panferov, O. Modification of two-equation models to account for plant drag. Bound. Layer Meteorol. 121, 229-266 (2006).

Sogachev, A., Kelly, M. & Leclerc, M. Consistent two-equation closure modelling for atmospheric research: buoyancy and vegetation implementations. Bound. Layer Meteor. 145, 307-327 (2012).

Twomey S. The influence of pollution on the shortwave albedo of clouds. J. Atmos. Sci. 34, 1149-1152. (1997)

Zhou, L. et al. Contribution from biogenic organic compounds to particle growth during the 2010 BEACHON-ROCS campaign in a Colorado temperate needle leaf forest. Atmos. Chem. Phys. Discuss. 15, 9033-9075 (2015).

Zhou, L. et al. SOSAA - a new model to simulate the concentrations of organic vapours, sulphuric acid and aerosols inside the ABL - Part 2: Aerosol dynamics and one case study at a boreal forest site. Boreal Environ. Res. 19, 237-256 (2014).

B3 Scaling of silver birch stand radiative forcing related to secondary organic aerosols

Published measurements of the emissions of VOCs from birch are rare. Yli-Pirilä et al. (2016) measured the VOC emissions from both mountain birch and silver birch seedlings in the laboratory. They found that the emissions of monoterpenes were very similar for the two species, though statistically slightly lower from silver birch and the maximum monoterpene leaf scale emission rate was 1.1 $\mu g\ g^{-1}\ h^{-1}$ (when standardised to photosynthetic photon flux density PPFD=1000 $\mu mol\ m^{-2}\ s^{-1}$ and T=30ºC). Vuorinen et al. (2007) report monoterpene emission rates of 1.01-1.49 $\mu g\ g^{-1}\ h^{-1}$ (PPFD =1000 $\mu mol\ m^{-2}\ s^{-1}$, T=30°C) for sapling silver birches measured in the laboratory. Two years old silver birch seedlings measured in the laboratory during September was shown to emit monoterpenes with a rate of 1.63 $\mu g\ g^{-1}\ h^{-1}$ (PPFD =1000 $\mu mol\ m^{-2}\ s^{-1}$, T=30°C, assuming a leaf mass area of 90 g m^{-2}) (Ghirado et al., 2010). Maja et al. (2014) measured the emission of VOCs from potted silver birch saplings in the field. The emission factor for monoterpenes varied from 0.015-0.4 $\mu g\ g^{-1}\ h^{-1}$ (when assuming a leaf mass area of 90 g m^{-2} and when standardised to 30°C, but under varying and unknown light conditions), depending on the individual clone and specific time during the growing season. Though the focus of most of the above mentioned papers has been on comparing control plant emissions to those of biotically stressed plants, the emission potentials mentioned in this section are purely for healthy plants. Hence, previous laboratory measurements show two things: i) firstly that the emission rate of monoterpenes from healthy unstressed birch is significant and in the same range as the emissions from spruce and pine (Taipale et al., 2011, Aalto et al., 2014, Rantala et al., 2015, Hakola et al., 2017), ii) and secondly that there is a large variability in the observed emission potentials. To our knowledge, there currently only exist two published papers on the emission of VOCs from young silver birch saplings in the ***field*** (Hakola et al. 1998, 2001). Hakola et al. (1998, 2001) conducted measurements throughout the growing season and suggested a monoterpene emission potential from silver birch that depends on the effective temperature sum (ETS) in order to capture the seasonal dependency on the emission potential. Hakola et al. (2001) provided no information on the light conditions in the field, though Hakola et al. (1998) reported that PPFD is usually slightly higher than 1000 $\mu mol\ m^{-2}\ s^{-1}$. Since the emission of monoterpenes was historically only described as volatilisation from storage pools, Hakola et al. (2001) only standardised the emission with respect to temperature (30°C), and not light. The monoterpene emission potential is $3.68 \pm 0.38\ \mu g\ g^{-1}\ h^{-1}$ when ETS < 80°C and only based on two measurement points; $0.68 \pm 0.57\ \mu g\ g^{-1}\ h^{-1}$ when 80°C < ETS < 400°C and $7.71 \pm 4.64\ \mu g\ g^{-1}\ h^{-1}$ when ETS > 400°C. For comparison, the laboratory values measured by Yli-Pirilä et al. (2016), Ghirardo et al. (2010) and Vuorinen et al. (2007) are similar or up to more than a factor of two higher than Hakola et al. (2001) when 80°C < ETS < 400°C, but less than half of Hakola et al. (2001) when ETS < 80°C. Hence, laboratory and field measurements agree relatively well on the emission potentials in the beginning of the growing season, but not later on. Since laboratory experiments cannot reproduce the effects of the many environmental factors that simultaneously affect the rate of emission - even environmental factors that do not stress the plants - and cannot capture the impacts of seasonality, we utilised Hakola et al. (2010)'s emission potential for atmospheric simulations of birch. However, very recent continuous field measurements (unpublished and preliminary results) obtained after completion of SOSAA simulations and radiative forcing calculations, suggest that the canopy scale emissions of monoterpenes from silver birch based on Hakola et al. (2001) could be highly overestimated. The overestimation in Hakola et al. (2001)'s late season emission potential is most probably caused by the method, which has fortunately drastically improved during the past 20 years. Hakola et al. (2001) enclosed branches in teflon bags for ~1 h, which caused the temperature to rise very significantly above the ambient and hence altered the emission rate drastically. Additionally, measurements were

always conducted on new leaves, hence late season measurements were obtained on leaves from the second leaf flush, which firstly only makes up a minority of the total canopy foliage – at least in Finland, and secondly might have different emission potentials due to better growing conditions later in the summer. In our simulations of year 2010 climate, ETS > 400°C is reached in the end of June, and hence we presume that the predicted number and size of aerosol particles during July – September are overestimated. Due to these uncertainties we downscaled the number and size of aerosol particles from birch stands during July – September and reduced the impact of monoterpene emissions from silver birch on atmospheric aerosol processes and the radiative forcing caused by these particles.

The downscaling was conducted as follows: The emission potential of 7.71 μg g^{-1} h^{-1} was reduced to 0.68 μg g^{-1} h^{-1}, where we assume that the leaves sustained the same emission potential both before and after ETS > 400°C, and that the emission rate only depends on temperature. When the emission is only assumed to depend on temperature, the canopy scale emission during unchanging temperature conditions (we use same ambient temperature for birch, spruce and pine, so the activity coefficient is same for them all), can roughly be expressed as: canopy scale emission ∝ emission factor * biomass, since the temperature difference between shaded and sunlit leaves is small and sometimes even neglected in models (e.g. Simpson et al., 2012). Hence we matched the product of the reduced emission factor and biomass of the birch stands, with those of the pine and spruce stands (see Table S3). Hence, the aerosol RF of individual birch stands was downscaled to the RF of the conifer stand with which it was matched. Though the route from the emission of VOCs, through atmospheric chemistry, to new particle formation and growth is highly non-linear, this scaling still serves as a reasonable approximation. Sensitivity tests show that if the same chemotype is assumed, then an increase in the emission of monoterpenes leads to a similar increase in the concentration of OH and pinonic acid, even if the increase is very significant (Bäck et al., 2017). One obstacle for the scaling using the emission of other tree species is the diversity in the emitted blend of monoterpenes, because they impact the atmospheric chemistry and aerosol processes differently. However, little is known of the emitted spectrum of monoterpenes from various plant species, and individual genotypes have also been shown to emit very different proportions of individual monoterpenes (Bäck et al. 2012). In reality, the emission of VOCs from silver birch depends not only on temperature, but also light (Ghirardo et al., 2010), and our recent continuous field measurements (which we referred to earlier) show that the canopy scale emission is higher than what is predicted by an emission factor of 0.68 μg g^{-1} h^{-1}, but as mentioned earlier, significantly less than 7.71 μg g^{-1} h^{-1}. Hence the aerosol RF based on the SOSAA simulations should be viewed as the upper limit, while our scaled values should be viewed as the lower limit.

Supplementary Table S3 Emission factors and emission factors multiplied with biomass of different species. Last column shows which conifers species and the age of those stands to which radiative forcing of silver birch aerosols were downscaled.

Species	Age (years)	Emission factor (μg/g/h)	Emission factor * biomass (μg/h/cm^2)	Scaled to
Birch	10	0.68	0.00419	**Spruce, 15 years**
	20		0.0195	**Spruce, 50 years**
	50		0.0133	**Pine, 15 years**
Spruce	15	0.12 (June) 0.25 (July) 0.16 (Aug) 0.08 (Sep)	0.00817 (June) 0.0170 (July) 0.0109 (Aug) 0.00544 (Sep)	
	30		0.0160 (June) 0.0334 (July) 0.0214 (Aug) 0.0107 (Sep)	
	50		0.0147 (June) 0.0306 (July) 0.0196 (Aug) 0.00978 (Sep)	
Pine	15	0.48 (June, mean) 0.82 (July, mean) 0.62 (Aug, mean) 0.26 (Sep, mean)	0.00930 (June) 0.0159 (July) 0.0120 (Aug) 0.00508 (Sep)	
	20		0.0247 (June) 0.0422 (July) 0.0319 (Aug) 0.0135 (Sep)	
	50		0.0242 (June) 0.0413 (July) 0.0311 (Aug) 0.0132 (Sep)	

References:

Aalto, J., Kolari, P., Hari, P., Kerminen, V.-M., Schiestl-Aalto, P., Aaltonen, H., Levula, J., Siivola, E., Kulmala, M., and Bäck, J.: New foliage growth is a significant, unaccounted source for volatiles in boreal evergreen forests, Biogeosciences, 11, 1331–1344, https://doi.org/10.5194/bg-11-1331-2014, 2014.

Bäck, J., Aalto, J., Henriksson, M., Hakola, H., He, Q., and Boy, M.: Chemodiversity of a Scots pine stand and implications for terpene air concentrations, Biogeosciences, 9, 689–702, https://doi.org/10.5194/bg-9-689-2012, 2012.

Bäck, J., Taipale, D., and Aalto, J. Deciduous birch canopy as unexpected contributor to stand level atmospheric reactivity in boreal forests. Geophysical Research Abstracts Vol. 19, EGU2017-16653, 2017 EGU General Assembly 2017.

Ghirardo, A. Koch, K., Taipale, R., Zimmer, I., Schnitzler, J.-P. And Rinne, J. Determination of de novo and pool emissions of terpenes from four common boreal/alpine trees by 13CO2 labelling and PTR-MS analysis. Plant, Cell and Environment. 2010; Vol. 33, No. 5. pp. 781-792.

Hakola, H., Rinne, J., and Laurila, T.: The hydrocarbon emission rates of tea-leafed willow (Salix phylicifolia), silver birch (Betula pendula) and European aspen (Populus tremula), Atmos. Environ., 32, 1825–1833, https://doi.org/10.1016/S1352-2310(97)00482-2, 1998.

Hakola, H., Laurila, T., Lindfors, V., Hellén, H., Gaman, A., and Rinne, J.: Variation of the VOC emission rates of birch species during the growing season, Boreal Env. Res., 6, 237–249, 2001.

Hakola, H., Tarvainen, V., Praplan, A. P., Jaars, K., Hemmilä, M., Kulmala, M., Bäck, J., and Hellén, H.: Terpenoid and carbonyl emissions from Norway spruce in Finland during the growing season, Atmos. Chem. Phys., 17, 3357-3370, https://doi.org/10.5194/acp-17-3357-2017, 2017.

Maja, M. M., Kasurinen, A., Yli-Pirilä, P., Joutsensaari, J., Klemola, T., Holopainen, T., and Holopainen, J. K.: Contrasting responses of silver birch VOC emissions to short- and long-term herbivory, Tree Physiology 34, 241-252, https://doi.org/10.1093/treephys/tpt127, 2014.

Rantala, P., Aalto, J., Taipale, R., Ruuskanen, T. M., and Rinne, J.: Annual cycle of volatile organic compound exchange between a boreal pine forest and the atmosphere, Biogeosciences, 12, 5753–5770, https://doi.org/10.5194/bg-12-5753-2015, 2015.

Simpson, D., Benedictow, A., Berge, H., Bergström, R., Emberson, L. D., Fagerli, H., Flechard, C. R., Hayman, G. D., Gauss, M., Jonson, J. E., Jenkin, M. E., Nyíri, A., Richter, C., Semeena, V. S., Tsyro, S., Tuovinen, J.-P., Valdebenito, Á., and Wind, P.: The EMEP MSC-W chemical transport model – technical description, Atmos. Chem. Phys., 12, 7825-7865, https://doi.org/10.5194/acp-12-7825-2012, https://doi.org/10.5194/acp-12-7825-2012, 2012.

Taipale, R., Kajos, M. K., Patokoski, J., Rantala, P., Ruuskanen, T. M., and Rinne, J.: Role of de novo biosynthesis in ecosystem scale monoterpene emissions from a boreal Scots pine forest, Biogeosciences, 8, 2247–2255, https://doi.org/10.5194/bg-8-2247-2011, 2011.

Vuorinen, T., Nerg, A.-M., Syrjälä, L., Peltonen, P., and Holopainen, J. K.: Epirrita autumnata induced VOC emission of silver birch differ from emission induced by leaf fungal pathogen, Arthropod-Plant Inte., 1, 159-165, https://doi.org/10.1007/s11829-007-9013-4, 2007.

B4 Stand level radiative forcing dynamics of CO_2, SOA, albedo and subsitution

The CO_2 effect at the stand level combined stand increment, soil carbon, harvest impact and decay of wood products. We calculated the decay of CO_2 pulse with parameters showed in Table S4 and Fig. S12 shows the evolvement of function state variables in Scots pine stand.

Supplementary Table S4 Parameter values used in CO_2 life time function (IPCC 2007).

Parameter	Value
α0	0,217
α1	0,259
α2	0,338
α3	0,186
τC,1	172,9
τC,2	18,5
τC,3	1,2

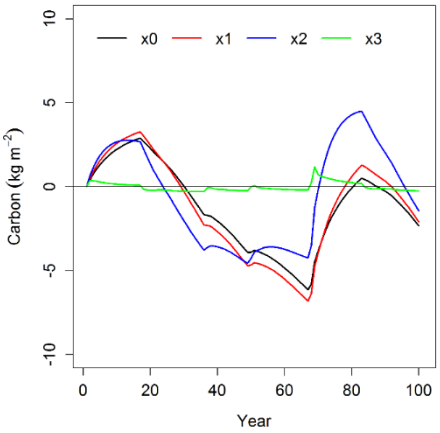

Supplementary Figure S12 Temporal dynamics of state variables describing different independent reservoirs removing CO_2 from atmosphere (IPCC 2007). In this example, we used 100 years simulation of a Scots pine stand as an input for this CO_2 life-time function. Simulated forest management, i.e. thinnings and final harvest, followed recommendations and state variables x0…x3 were calculated with corresponding parameter values in Table S4.

Concerning also the biophysical effects, the different effects had different dynamics with respect of forest development (Fig. S13). Harvesting caused an increase in RF due to the loss of carbon sequestration and a decrease in SOA, but a decrease due to an increase in substitution and also in albedo in the conifers. The deciduous silver birch stand's albedo had an opposite effect to that of the conifer stand's, being slightly higher than the open area albedo, i.e. clear cut had a warming effect in terms of albedo in silver birch. In the SOA effect, the increased cloud albedo due to forest VOCs dominated since direct RF effect of aerosol particles ranged only from 3% to 6% in different species (data not shown). The SOA-induced cooling of closed canopy forest relative to the reference clearcut

was comparable to that caused by carbon sequestration over stand rotation. Although the maximum cooling by SOA over rotation was lower than that of cumulative carbon sequestration, the average cooling was comparable since the SOA effect tracked the size of the canopy whereas the carbon effect followed biomass accumulation in trees, litter and harvested wood products. For the coniferous species, the SOA induced cooling exceeded the warming induced by low albedo of forest cover under the present climate.

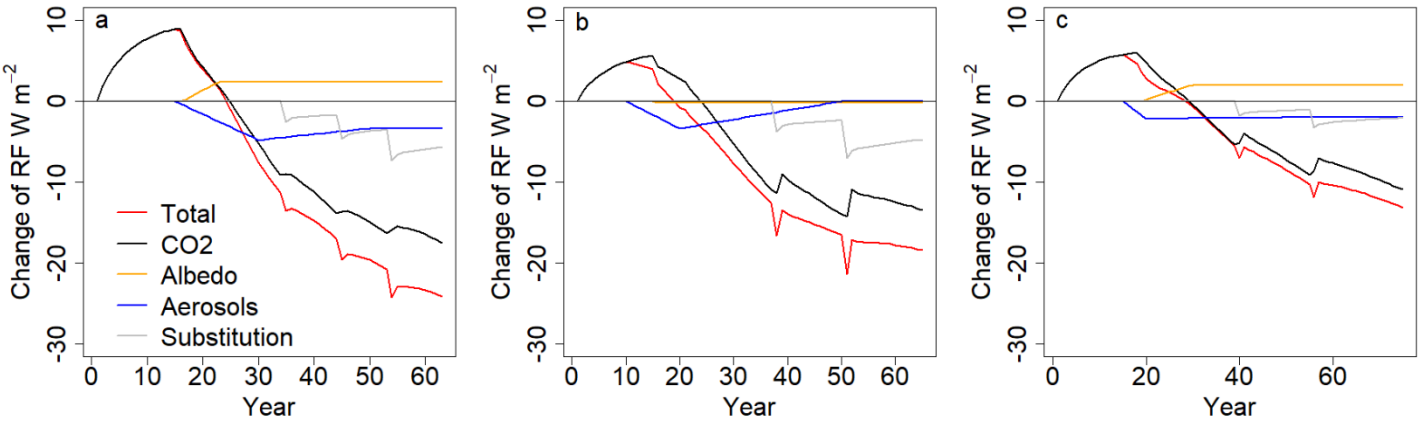

Supplementary Figure S13 The dynamic local radiative forcing (RF) caused by CO_2 sequestration in forest stands and wood products (CO_2), surface albedo (A), aerosols (SOA) and avoided emissions from the use of wood products (substitution) per unit area (m^2) for silver birch, Norway spruce and Scots pine stands over one rotation in the present climate when the stands are managed according to recommended rotation lengths and management options. The curves show the change relative to RF at the initial state along stand development dynamics, i.e. how different forcing agents change along the vegetation dynamics relative to the clear cut area until final cut and growth of next tree generation. The thinnings during rotation period are shown as dips in curves. Aerosol forcing did not change during first 15 years after clear cut in spruce and pine, and 10 years in birch, because clearcut areas were not simulated.

B5 The effect of climate change

To analyse forest growth and carbon sequestration under climate change, the process-based models OptiPipe (Mäkelä et al. 2008b) and PRELES (Mäkelä et al. 2008a) were used. In the OptiPipe model, tree volume growth was obtained through the allocation of gross primary production (GPP) depending on the carbon:nitrogen ratio, temperature sum and soil nitrogen availability. Soil nitrogen availability increases concurrently with the increasing temperature sum. The potential increase of soil nitrogen availability was set higher in simulations for fertile forest sites than for poorer sites (Mäkelä et al. 2008b). The GPP prediction in PRELES is based on the concept of light use efficiency. The model uses daily values for the absorbed photosynthetically active radiation (aPAR) and modifiers for atmospheric CO_2 concentration, light, temperature, vapor pressure, soil water and phenological state for GPP calculation (Peltoniemi et al. 2015). The obtained relative changes in volume growth were used to modify the growth functions of MOTTI for the 2050 climate. The GPP potential of Finnish forests, used as an input in OptiPipe, was estimated using PRELES for the mean climate model projections of a climate emission scenario between RCP6.0 and RCP8.5 scenarios (Rogelj et

al. 2012) for the year 2050. The constructed climate scenario combined a daily observed data set on a 10 x 10 km grid over Finland with changes in the long-term average, simulated by an ensemble of 8 Global Circulation Models (GCM) up to year 2050. The development of atmospheric CO_2 concentration during 21st century was obtained from the BERN carbon cycle model (IPCC 2013). Details of the construction of climate scenarios are described by Rötter et al. (2013) and Kalliokoski et al. (2018).

Under the 2050 climate, the SOA effect over stand rotation was larger than in the current climate (from -2.3 to -5.4 Wm^{-2} for the herb rich spruce site type) due to enhanced BVOC emissions and subsequent SOA formation, related to increased temperatures. This effect more than compensated for the increase in RF from reduced carbon sequestration (from -3.8 to -2.4 Wm^{-2}) due to more rapid biomass turnover (litter and soil carbon, also shorter stand rotation time) in the warmer climate.

The differences in RF between the harvest levels increased further under the 2050 climate. Largely due to changes in SOA forcing, the higher harvest rates had a bigger warming influence than in current climate, while change in the difference between the lowest harvest rates was minor (Fig. S14). In the 2050 climate analyses, the PS was not considered since it is a property of the technosphere (comprised of all of the structures that humans have constructed) and thus larger and more rapid changes in it could occur than in the forest related properties of biosphere.

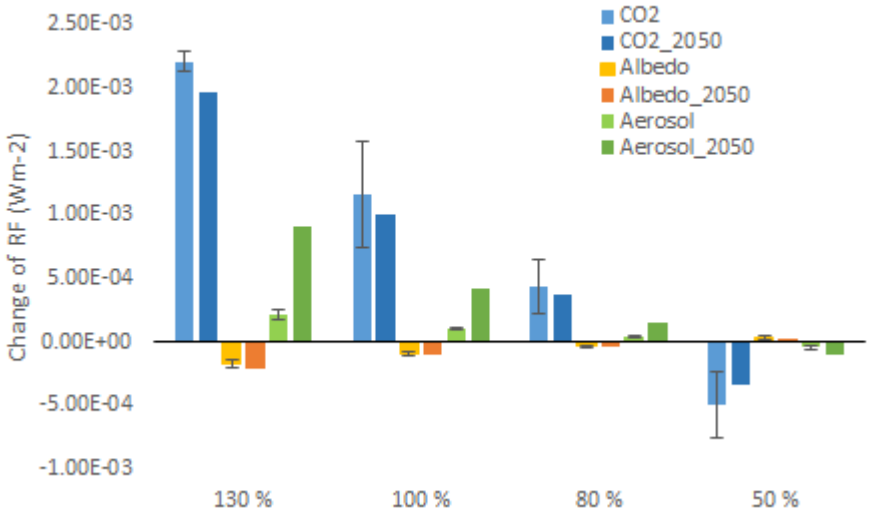

Supplementary Figure S14 Contribution of different factors to the average change of global radiative forcing (RF) in 50 years due to changes in Finnish forests in different harvest scenarios, expressed as difference from the baseline (65% current annual increment, CAI) in current and scenario climate. The scenario climate corresponds climatic conditions of year 2050. CO_2 includes carbon sequestered in trees, soil and forest products, 'Albedo' refers to the change in surface albedo, 'Aerosol' equals both direct and indirect effects of secondary organic aerosols. We did not calculate substitution in 2050. Positive values indicate warming, and negative values cooling effect. The error bars indicate the estimated min-max range in current climate.

References

IPCC, 2007. Climate change 2007: The Physical Science Basis. Contribution of Working Group I to the Fourth Assessment Report of the Intergovernmental Panel on Climate Change Group I to the Fourth Assessment Report of the Intergovernmental Panel on Climate Change Available at http://www.ipcc.ch.

IPCC, 2013. Climate Change 2013: The Physical Science Basis. Contribution of Working Group I to the Fifth Assessment Report of the Intergovernmental Panel on Climate Change. F. T. Stocker et al. Eds. (Cambridge Univ. Press, Cambridge, 2013), pp. 1535.

Kalliokoski, T., Mäkelä, A., Fronzek, S., Minunno, F., Peltoniemi, M. Decomposing sources of uncertainty in climate change projections of boreal forest primary production. Agric. For. Meteorol. 262, 192–205, 2018, https://doi.org/10.1016/J

Mäkelä, A., Pulkkinen, M., Kolari, P., Lagergren, F., Berbigier, P., Lindroth, A., Loustau, D., Nikinmaa, E., Vesala, T. and Hari, P.: Developing an empirical model of stand GPP with the LUE approach: analysis of eddy covariance data at five contrasting conifer sites in Europe, Glob. Chang. Biol., 14, 92-108, 2008a.

Mäkelä, A., Valentine, H. T. and Helmisaari, H. S.: Optimal co-allocation of carbon and nitrogen in a forest stand at steady state, New Phytol., 180, 114-123, 2008b.

Peltoniemi, M., Pulkkinen, M., Aurela, M., Pumpanen, J., Kolari, P. and Mäkelä, A.: A semi-empirical model of boreal forest gross primary production, evapotranspiration, and soil water – calibration and sensitivity analysis, Bor. Env. Res., 20, 151-171, 2015.

Rogelj, J., Meinshausen, M., Knutti, R., Global warming under old and new scenarios using IPCC climate sensitivity range estimates, Nat. Clim. Change, 2, 248-253, 2012.

Rötter, R. P., Höhn, J., Trnka, M., Fronzek, S., Carter, T.R. and Kahiluoto, H.: Modelling shifts in agroclimate and crop cultivar response under climate change, Ecol. Evol., 3, 4197 – 4214, 2013.